

Numerical Homogenization of Landau-Lifshitz Equation with Rough Coefficients

Zetao Ma¹, Jingrun Chen^{2,3}, Rui Du^{4,5,*}, and Lei Zhang^{1,6,7}

¹ School of Mathematical Sciences, Shanghai Jiao Tong University, Shanghai 200240, P.R. China.

² School of Mathematical Sciences, University of Science and Technology of China, Hefei, Anhui 230026, P.R. China.

³ Suzhou Institute for Advanced Research, University of Science and Technology of China and Suzhou Big Data & AI Research and Engineering Center, Suzhou, Jiangsu 215123, P.R. China.

⁴ School of Mathematical Sciences, Soochow University, Suzhou, 215006, P.R. China.

⁵ Mathematical Center for Interdisciplinary Research, Soochow University, Suzhou, 215006, P.R. China.

⁶ Institute of Natural Sciences, Shanghai Jiao Tong University, Shanghai 200240, P.R. China.

⁷ MOE-LSC, Shanghai Jiao Tong University, Shanghai 200240, P.R. China.

Abstract. In this work, we develop a numerical homogenization approach for the fully nonlinear Landau-Lifshitz equation with rough coefficients, including non-periodicity and nonseparable scales. Direct numerical resolution of such multiscale problems on fine meshes incurs prohibitive computational costs. To address this challenge, we propose an efficient coarse scale approximation through localized basis functions derived from energy minimization within the Generalized Rough Polyharmonic Splines (GRPS) framework. These basis functions preserve critical multiscale features while operating on a computationally tractable coarse mesh. The nonlinear, vectorial, and non-symmetric nature of the Landau-Lifshitz equation necessitates careful design of variational formulations for basis construction. We introduce several such formulations, each tailored to specific structural aspects of the problem. Through systematic numerical experiments, we demonstrate that our approach achieves significant computational savings without compromising accuracy, offering a robust framework for simulating multiscale magnetic systems with complex microstructures.

AMS subject classifications: 41A15, 65K10, 78M40, 82D40

Key words: numerical homogenization, generalized rough polyharmonic splines, multiscale finite element method, computational micromagnetism, Landau-Lifshitz equation.

*Corresponding author. Email addresses: 770120068@qq.com (Z. Ma), jingrunchen@ustc.edu.cn (J. Chen), durui@suda.edu.cn (R. Du), and lzhang2012@sjtu.edu.cn (L. Zhang)

1 Introduction

The magnetization dynamics in a ferromagnetic material is characterized by the Landau-Lifshitz (LL) equation [35, 43] for the magnetization $\mathbf{m} : \Omega \times (0, T] \rightarrow \mathbb{R}^3$, which assumes the following dimensionless form,

$$\begin{cases} \partial_t \mathbf{m} = -\mathbf{m} \times \mathbf{h}_{\text{eff}} - \lambda \mathbf{m} \times (\mathbf{m} \times \mathbf{h}_{\text{eff}}), & \mathbf{x} \in \Omega, t \in (0, T], \\ \kappa(\mathbf{x}) \frac{\partial \mathbf{m}}{\partial \mathbf{n}} = \mathbf{0}, & \mathbf{x} \in \partial\Omega, t \in (0, T], \\ \mathbf{m}(\mathbf{x}, 0) = \mathbf{m}_0(\mathbf{x}), & \mathbf{x} \in \Omega, \end{cases} \quad (1.1)$$

where $\Omega \subseteq \mathbb{R}^d$, $d=2,3$, is a bounded, smooth, and convex spatial domain. The parameter $\lambda > 0$ represents the dimensionless damping parameter, indicating the magnitude of the damping effect, and the initial data \mathbf{m}_0 satisfies $|\mathbf{m}_0| = 1$ in the point-wise sense. The vector \mathbf{n} represents the outward unit normal to the boundary $\partial\Omega$. The effective field \mathbf{h}_{eff} combines the exchange and anisotropic terms, and is given by

$$\mathbf{h}_{\text{eff}}[\mathbf{m}] = \underbrace{\text{div}(\kappa \nabla \mathbf{m})}_{\text{exchange term}} - \underbrace{(\mathbf{m} - (\mathbf{m} \cdot \mathbf{u})\mathbf{u})}_{\text{anisotropic term}}, \quad (1.2)$$

where the exchange parameter $\kappa(\mathbf{x})$ consists of rough coefficients (i.e., $\kappa \in L^\infty$), such that

$$\kappa_{\min} |\xi|^2 \leq \xi^T \kappa(\mathbf{x}) \xi \leq \kappa_{\max} |\xi|^2, \quad (1.3)$$

for all $\xi \in \mathbb{R}^d$ and almost every $\xi \in \Omega$. The material dependence of the exchange parameters varies at a very small scale and may not rely on concepts of ergodicity or scale separation, such as in high performance rare-earth magnetic alloys [36]. Studying these materials is challenging due to their strong heterogeneity and highly nonlinear nature. Additionally, we denote the anisotropy energy density as

$$\mathbf{m}_a = \mathbf{m} - (\mathbf{m} \cdot \mathbf{u})\mathbf{u} = (0, m_2, m_3)^T \quad (1.4)$$

with $\mathbf{m} = (m_1, m_2, m_3)^T$ and $\mathbf{u} = (1, 0, 0)^T$ (i.e., along the X-axis) for a uniaxial material. The Landau-Lifshitz energy functional is defined as

$$F[\mathbf{m}] = \frac{1}{2} \int_{\Omega} (\kappa |\nabla \mathbf{m}|^2 + (|\mathbf{m}|^2 - |\mathbf{m} \cdot \mathbf{u}|^2)) \, d\mathbf{x} = -\frac{1}{2} (\mathbf{h}_{\text{eff}}[\mathbf{m}], \mathbf{m}), \quad (1.5)$$

where the first equality indicates that $F[\mathbf{m}]$ is positive, and due to the minus sign ensures the non-positivity of \mathbf{h}_{eff} .

Several papers have analyzed the homogenization of the LL model from the analytical perspective, where $\kappa(x)$ can be expressed as $\kappa(x) = a(\frac{x}{\varepsilon})$, $a(x, \frac{x}{\varepsilon})$, or $a(\frac{x}{\varepsilon}, \omega)$, showcasing various scale separation characteristics [4, 5, 16, 18, 44, 47, 62]. In cases with scale separation ($\varepsilon \ll 1$) such that $\kappa(x) = a^\varepsilon$, the heterogeneous multiscale method (HMM) computes the homogenized solution using microscopic cell problems, reducing the computational

burden associated with resolving fine scales [45, 46, 48]. However, these models overlook the exchange term with rough coefficients, which is a more practical scenario [36], and cannot be effectively addressed by numerical methods based on the scale separation assumption.

To date, numerical homogenization without scale separation has matured for benchmark problems such as elliptic PDEs. Key methods include asymptotic homogenization [41, 59], numerical homogenization [2, 26, 64], heterogeneous multiscale methods [1, 27, 28], multiscale network approximations [10], multiscale finite element methods (MsFEM) [8, 30, 31], variational multiscale methods [9, 40], flux norm homogenization [11, 56], rough polyharmonic splines (RPS) and its generalization (GRPS) [50, 54, 58], localized orthogonal decomposition (LOD) [6, 37, 53], and generalized multiscale finite element methods (GMsFEM) [19–21, 29, 51].

In this work, we employ RPS/GRPS as our primary numerical homogenization approach. These methods have proven effective for obtaining accurate multiscale solutions to elliptic, parabolic, and hyperbolic equations [50, 55–58]. The GRPS method, as developed in [50], incorporates multiple energy forms and measurement functions (edge, volume, and derivative measurements). Specifically, the edge-based GRPS (GRPS-E) achieves first-order accuracy in the H^1 sense for $g \in L^2(\Omega)$, while both volume-based (GRPS-V) and derivative-based (GRPS-D) approaches attain second-order accuracy when $g \in H^1(\Omega)$.

The Landau-Lifshitz equation (1.1) presents several unique challenges beyond standard linear PDEs:

- **Nonlinearity:** The terms $-\mathbf{m} \times \mathbf{h}_{\text{eff}} - \lambda \mathbf{m} \times (\mathbf{m} \times \mathbf{h}_{\text{eff}})$ exhibit third-order nonlinearity. Various temporal discretization approaches [3, 15, 23, 24, 34, 42, 60, 65] have been developed, ranging from explicit (with strict stability constraints) to fully implicit (requiring expensive nonlinear solves) and semi-implicit schemes (offering better stability-efficiency balance). These choices directly affect the resulting bilinear forms in numerical homogenization.
- **Skew-symmetry:** The term $-\mathbf{m} \times \mathbf{h}_{\text{eff}}$ introduces a skew-symmetric component to the bilinear form, necessitating a generalized Lax-Milgram framework [17].
- **Vectorial nature:** As a 3-component vectorial PDE, the LL equation triples the system dimensionality. The bilinear form can be constructed either as a combined variational form or as separate forms for each component.
- **Constraint preservation:** The magnetization constraint $|\mathbf{m}| = 1$ is typically maintained through point-wise projection, though well-designed schemes can preserve this property without explicit projection.

While numerical homogenization has been successfully applied to nonlinear PDEs [38, 39, 49, 52, 63], vectorial problems (e.g., $H(\text{curl})$ -systems) [33], and non-symmetric prob-

lems (e.g., convection-dominated systems) [12, 13, 32], this work represents the first application to the LL equation incorporating all these features simultaneously.

Using GRPS, we construct low-dimensional, operator-adapted basis functions with exponential decay, though LOD and GMsFEM remain viable alternatives. Through systematic investigation of different GRPS formulations (including bilinear forms, measurement functions, time discretizations, and anisotropy terms), we identify optimal configurations exhibiting varying convergence rates, including higher-order convergence.

The paper is organized as follows: Section 2 overviews FEM approaches for the LL equation; Section 3 details GRPS basis derivation and reduced-space approximation; Section 4 presents numerical experiments validating our method's accuracy and efficiency; and Section 5 provides concluding remarks.

Notation: (\cdot, \cdot) represents L^2 -inner product in space.

2 Numerical Methods for Model Problem

The LL equation has been extensively studied using conventional numerical methods such as finite difference and finite element approaches. For comprehensive reviews of these standard techniques, we refer readers to [15, 23, 42].

In our work, we focus on semi-implicit time discretization schemes [3, 14, 24, 34, 60, 65], which offer a practical balance between numerical stability and computational efficiency. We consider a uniform partition of the time interval $[0, T]$ denoted by $0 = t_0 < t_1 < \dots < t_N = T$, where the time step size is given by $\Delta t = T/N$. At each time step, these schemes require solving for the updated magnetization field $\mathbf{m}^{n+1} \in \mathbf{V} := [H^1(\Omega)]^3$ through the variational formulation:

$$A^n(\mathbf{m}^{n+1}, \mathbf{v}) = (\mathbf{f}^n, \mathbf{v}), \quad \forall \mathbf{v} \in \mathbf{V}. \quad (2.1)$$

The bilinear form A^n can be decomposed into two components that will be specified later,

- $B^n(\mathbf{m}^{n+1}, \mathbf{v})$: Contains the essential multiscale structure and heterogeneity of the problem, which plays a crucial role in defining our coarse approximation space V_H (where H represents the coarse scale parameter);
- $C^n(\mathbf{m}^{n+1}, \mathbf{v})$: Handles the linearized approximation of nonlinear terms, which as noted in [25], often has secondary importance when constructing the coarse space.

The presence of rough coefficients $\kappa(x)$ with fine-scale (characterized by length scale $0 < \epsilon \ll 1$) variations makes direct numerical simulation computationally prohibitive using conventional methods. This motivates our primary focus on developing an effective coarse space construction that can capture the essential multiscale behavior without resolving all fine-scale details.

2.1 Time Discretization Schemes

Using the fundamental constraint $|\mathbf{m}| = 1$ of micromagnetics, we can reformulate the LL equation (1.1) into an equivalent form that is often more amenable to discover the bilinear form:

$$\mathbf{m}_t - \lambda \mathbf{h}_{\text{eff}} + \mathbf{m} \times \mathbf{h}_{\text{eff}} = -\lambda (\mathbf{m} \cdot \mathbf{h}_{\text{eff}}) \mathbf{m} \quad (2.2)$$

Several semi-implicit backward Euler-type schemes have been developed to handle the nonlinear terms while maintaining $O(\Delta t + h^2)$ accuracy in the L^2 norm. These schemes all share a common structure for the B^n component of the bilinear form:

$$B^n(\mathbf{m}^{n+1}, \mathbf{v}) := \lambda (\kappa \nabla \mathbf{m}^{n+1}, \nabla \mathbf{v}) + \lambda (\mathbf{m}_a^{n+1}, \mathbf{v}) - (\mathbf{m}^n \times \kappa \nabla \mathbf{m}^{n+1}, \nabla \mathbf{v}) \quad (2.3)$$

while differing in their treatment of the remaining terms:

- **Cimrák's scheme** [23]:

$$\begin{aligned} C_{\text{Cimrak}}^n(\mathbf{m}^{n+1}, \mathbf{v}) &= \frac{1}{\Delta t} (\mathbf{m}^{n+1}, \mathbf{v}) - (\mathbf{m}^n \times \mathbf{m}_a^{n+1}, \mathbf{v}) + \lambda (\mathbf{m}^n \cdot \mathbf{h}_{\text{eff}}^{n+1}, \mathbf{v}), \\ (\mathbf{f}_{\text{Cimrak}}^n, \mathbf{v}) &= \frac{1}{\Delta t} (\mathbf{m}^n, \mathbf{v}); \end{aligned}$$

- **Gao's scheme** [34]:

$$\begin{aligned} C_{\text{Gao}}^n(\mathbf{m}^{n+1}, \mathbf{v}) &= \frac{1}{\Delta t} (\mathbf{m}^{n+1}, \mathbf{v}) - (\mathbf{m}^n \times \mathbf{m}_a^{n+1}, \mathbf{v}), \\ (\mathbf{f}_{\text{Gao}}^n, \mathbf{v}) &= -\lambda ((\mathbf{m}^n \cdot \mathbf{h}_{\text{eff}}^n) \mathbf{m}^n, \mathbf{v}) + \frac{1}{\Delta t} (\mathbf{m}^n, \mathbf{v}); \end{aligned}$$

- **An's scheme** [7]:

$$\begin{aligned} C_{\text{An}}^n(\mathbf{m}^{n+1}, \mathbf{v}) &= \frac{1}{\Delta t} (\mathbf{m}^{n+1}, \mathbf{v}) - (\mathbf{m}^n \times \mathbf{m}_a^{n+1}, \mathbf{v}) + \lambda ((\mathbf{m}^n \cdot \bar{\mathbf{h}}_{\text{eff}}^{n+1}) \cdot \mathbf{m}^n, \mathbf{v}), \\ (\mathbf{f}_{\text{An}}^n, \mathbf{v}) &= \frac{1}{\Delta t} (\mathbf{m}^n, \mathbf{v}). \end{aligned}$$

2.2 Numerical Homogenization Framework

To construct our coarse approximation space V_H , we employ the Generalized Rough Polyharmonic Splines (GRPS) method [50, 54, 58], which has proven effective for numerical homogenization of multiscale problems. The approach begins with the following setup:

- **Mesh structure:** Let \mathcal{T}_H be a coarse simplicial subdivision of the domain Ω into $2N_c^2$ parts with maximum element diameter H . \mathcal{T}_H can be uniformly refined J times to create a fine mesh \mathcal{T}_h with $h = 2^{-J}H$.

- **Function spaces:** On \mathcal{T}_h , we define the standard first-order conforming finite element space:

$$V_h = \{\varphi \in C^0(\Omega) \mid \varphi|_\tau \in \mathcal{P}_1(\tau), \forall \tau \in \mathcal{T}_h\} \subset H^1(\Omega)$$

with the vector-valued counterpart $\mathbf{V}_h = V_h^3$ for our LL equation application.

Consider the model elliptic problem $-\nabla \cdot (\kappa(x) \nabla u) = f$ where $\kappa \in L^\infty(\Omega)$ is bounded and positive definite. The associated bilinear form is:

$$B(u, v) = \int_{\Omega} \kappa(x) \nabla u \cdot \nabla v dx. \quad (2.4)$$

The numerical homogenization seeks a coarse space $V_H \subset V_h$ of dimension much smaller than V_h such that the coarse solution $u_H \in V_H$ satisfies:

$$B(u_H, v_H) = (f, v_H), \quad \forall v_H \in V_H \quad (2.5)$$

with an approximation error comparable to the coarse mesh size H .

2.2.1 GRPS Basis Construction

The GRPS approach constructs basis functions through the following procedure [50]:

1. Define N_H measurement functions $\{\phi_i\}_{i=1}^{N_H}$ (typically characteristic functions of coarse patches or edges);
2. For each ϕ_i , define the constrained space:

$$\mathcal{V}_i = \{\psi \in V_h \mid (\psi, \phi_j) = \delta_{ij}, j = 1, \dots, N_H\};$$

3. Solve the constrained minimization problem for each basis function:

$$\psi_i = \arg \min_{\psi \in \mathcal{V}_i} \|\psi\|_{B, \Omega}^2, \quad (2.6)$$

where $\|\psi\|_{B, \Omega} = \sqrt{B(\psi, \psi)}$ is the energy norm.

Remark 2.1. The choice of measurement functions significantly impacts both accuracy and computational efficiency. We focus on

- **Volume-based (GRPS-V):** Uses characteristic functions of coarse elements, with the set of measurement functions denoted as $\Phi_{\mathcal{T}}$;
- **Edge-based (GRPS-E):** Uses characteristic functions of coarse edges, with the set of measurement functions denoted as $\Phi_{\mathcal{E}}$.

They provide optimal balance between accuracy ($O(H)$ for $f \in L^2(\Omega)$) and reasonable number of degrees of freedom [50], while for GRPS-V we achieve higher accuracy $O(H^2)$ for $f \in H^1(\Omega)$.

2.2.2 Localization and Approximation Properties

While the exact GRPS basis functions $\{\psi_i\}$ possess global support, their exponential decay property permits effective localization through the following construction. First, let Ω_i^0 denote the nodal support of ψ_i . We then define the ℓ -layer patch Ω_i^ℓ as the ℓ -th order neighborhood of Ω_i^0 . The localized basis function ψ_i^ℓ is obtained by solving the constrained minimization problem

$$\psi_i^\ell = \underset{\substack{\psi \in \mathcal{V}_i \\ \text{supp}(\psi) \subset \Omega_i^\ell}}{\text{argmin}} \|\psi\|_{B, \Omega_i^\ell}^2, \quad (2.7)$$

where the minimization is performed over the subspace \mathcal{V}_i with support restricted to Ω_i^ℓ , and B represents the appropriate energy norm for the problem.

Theorem 2.1 (Localization Error [50, 58]). *For sufficiently large $\ell \geq C \log(1/H)$, the localized basis satisfies:*

1. *Exponential decay:*

$$\|\psi_i - \psi_i^\ell\|_{B, \Omega} \leq C_1 e^{-C_2 \ell} \|\psi_i\|_{B, \Omega};$$

2. *Approximation quality:*

$$\|u - u_H^\ell\|_{B, \Omega} \leq C(H^{s+1} + e^{-C_2 \ell}) \|f\|_{H^s(\Omega)}$$

for $s=0,1$, where u_H^ℓ is the solution in $\text{span}\{\psi_i^\ell\}$.

Remark 2.2. Recent developments in super-localization techniques [37] and LOD/SLOD methods [12, 13] offer promising alternatives, particularly for problems with additional structural challenges like strong convection or skew-symmetric terms. While we focus on GRPS for this work, these approaches present interesting directions for future research.

3 GRPS for the LL equation

In this section, we construct a coarse space for the bilinear form (2.1) by developing a multiscale basis for the magnetization components m_i ($i=1,2,3$). Solving (2.1) within this framework allows us to accurately capture the multiscale nature of the problem. This task is particularly challenging for the LL equation, as the bilinear form $B^n(\mathbf{m}^{n+1}, \mathbf{v})$ in (2.3) does not conform to a simple elliptic structure. Additionally, the choice of measurement function [50] plays a crucial role, as it can significantly influence convergence rates.

3.1 Construction of the Multiscale Basis Functions

The multiscale basis functions are constructed by solving the constrained minimization problem (2.6), representing the elliptic problem's energy norm. For the LL equation, the

bilinear form $B^n(\mathbf{m}, \mathbf{v})$ in (2.3) induces an energy norm equivalent (modulo λ) to the LL energy functional:

$$F[\mathbf{m}] = \frac{1}{2} \int_{\Omega} (\kappa |\nabla \mathbf{m}|^2 + (|\mathbf{m}|^2 - |\mathbf{m} \cdot \mathbf{u}|^2)) \, dx = -\frac{1}{2} (\mathbf{h}_{\text{eff}}[\mathbf{m}], \mathbf{m}),$$

as defined in (1.5).

Given measurement functions $\{\phi_j\}_{j=1}^{N_H} \subset \Phi$ ($\Phi = \Phi_{\mathcal{E}}$ or $\Phi_{\mathcal{T}}$), the GRPS basis solves:

$$\psi_i = \underset{\mathbf{m}}{\operatorname{argmin}} F[\mathbf{m}] \quad \text{s.t.} \quad \langle \phi_j, \mathbf{m} \rangle = \delta_{ij}, \quad \forall j.$$

The resulting GRPS space $V_H = \operatorname{span}\{\psi_i\}_{i=1}^{N_H}$ replaces the fine-scale space V_h on coarse meshes, and can apply to time discretization schemes such as (6.2), (6.3), (6.5).

To obtain the local GRPS basis space $\Psi^l = \operatorname{span}\{\psi_i^l\}$ within the local subdomain Ω_i^l , we solve the following optimization problem:

$$\left\{ \begin{array}{l} \psi_i^l = \underset{\mathbf{m}}{\operatorname{argmin}} F[\mathbf{m}] \\ \quad = \underset{\mathbf{m}}{\operatorname{argmin}} -\frac{1}{2} \int_{\Omega_i^l} \mathbf{h}_{\text{eff}}[\mathbf{m}] \cdot \mathbf{m} \, dx \\ \quad = \underset{\mathbf{m}}{\operatorname{argmin}} \frac{1}{2} \int_{\Omega_i^l} \kappa |\nabla \mathbf{m}|^2 + m_2^2 + m_3^2 \, dx, \\ \text{s.t.} \quad \langle \phi_j, \mathbf{m} \rangle = \delta_{ij}, \quad \forall \phi_j \in \Phi^l, \end{array} \right. \quad (3.1)$$

where Φ^l denotes the measurement functions in local patch Ω_i^l .

Remark 3.1. For the local optimization problem (3.1) on $\Omega_i^l \subsetneq \Omega$, homogeneous Dirichlet conditions hold on $\partial\Omega_i^l$ when $\Omega_i^l \subset \Omega$. For subdomains intersecting the global boundary ($\partial\Omega_i^l \cap \partial\Omega \neq \emptyset$), mixed conditions apply with Neumann on $\partial\Omega_i^l \cap \partial\Omega$ and Dirichlet on $\partial\Omega_i^l \setminus \partial\Omega$.

Given the vectorial nature of the equation and the anisotropy alignment $\mathbf{u} = (1, 0, 0)^T$, we solve two different variational problems from (3.1):

$$\left\{ \begin{array}{l} \psi_i^l = \underset{v}{\operatorname{argmin}} \int_{\Omega_i^l} \kappa |\nabla v|^2 \, dx \\ \text{s.t.} \quad \langle \phi_j, v \rangle = \delta_{ij}, \quad \forall \phi_j \in \Phi^l, \end{array} \right. \quad (V1)$$

$$\left\{ \begin{array}{l} \psi_i^l = \underset{v}{\operatorname{argmin}} \int_{\Omega_i^l} (\kappa |\nabla v|^2 + v^2) \, dx \\ \text{s.t.} \quad \langle \phi_j, v \rangle = \delta_{ij}, \quad \forall \phi_j \in \Phi^l. \end{array} \right. \quad (V2)$$

The basis from (V1) spans the GRPS space for m_1 , while (V2) generates the basis for m_2 and m_3 components, reflecting the magnetic-anisotropic energy structure.

Remark 3.2. Through the utilization of the energy minimization approach for the LL equation, there is no need to compute the multiscale basis at each time step. Besides, as documented in references [50, 58], an additional advantage of this method lies in the parallel computation of the multiscale basis, leading to significant savings in computational cost and time.

Exponential decay of multiscale basis functions We demonstrate the exponential decay properties of the multiscale basis functions through numerical experiments. The spatial domain $\Omega = [0,1]^2$ is partitioned into $N_c = 2^3$ patches, each subdivided into $J = 4$ segments, yielding a fine mesh size $h = 1/2^7$.

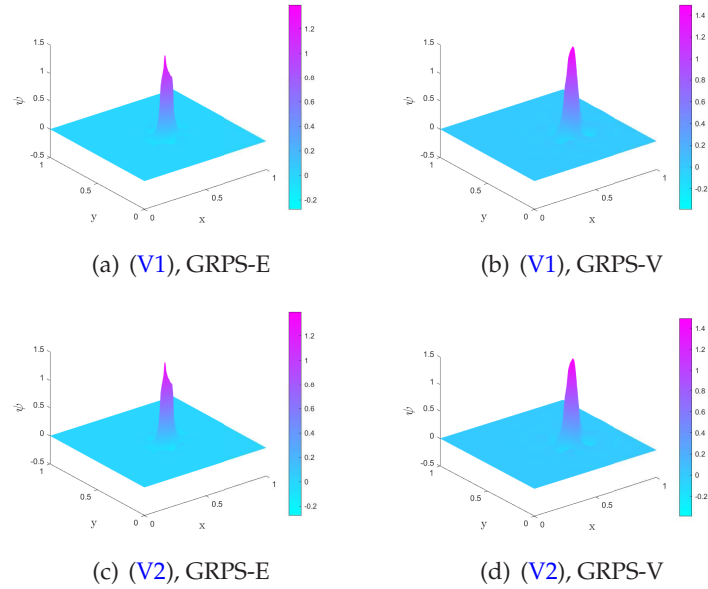


Figure 3.1: GRPS-E and GRPS-V basis functions obtained from $(V1)$ and $(V2)$.

Figures 3.1 and 3.2 display the profiles and decay characteristics of GRPS-E and GRPS-V basis functions derived from $(V1)$ and $(V2)$, with κ given by (4.2). The exponential decay is quantified by plotting $\log(\|\psi_i - \psi_i^l\| / \|\psi_i\|)$ against localization level l , confirming the expected decay behavior for both basis types.

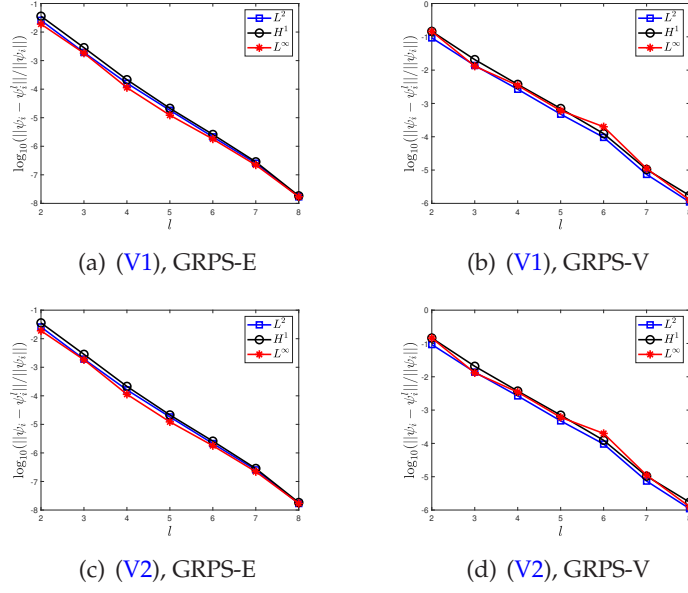


Figure 3.2: Exponential decay measured by $\|\psi_i - \psi_i^l\|/\|\psi_i\|$ in L^2 , H^1 , and L^∞ norms for localization levels $l = 2, \dots, 8$ (\log_{10} scale).

3.2 Multiscale Algorithms for Landau-Lifshitz Equation

With the coarse approximation space established, we now develop two distinct numerical approaches for solving the LL equation (2.2). The magnetization field \mathbf{m} in micromagnetics must theoretically satisfy the constraint $|\mathbf{m}| = 1$ at all points. While our first algorithm 1 relaxes this constraint, we demonstrate through numerical analysis [22, 34, 61] that careful discretization can maintain $|\mathbf{m}| \approx 1$ within controlled error bounds even without explicit enforcement. A *strict-constraint* approach (Algorithm 2) explicitly enforces $|\mathbf{m}| = 1$ at each computational step.

Algorithm 1 Multiscale length relaxing backward FEM for LL equation

- 1: Obtain the multiscale basis $\Psi = \{\psi_j\}_{j=1}^{N_H}$ by solving (3.1).
 - 2: Prescribe initial conditions: $\mathbf{m}_h^0, \mathbf{m}_H^0 = \sum_j \langle \phi_j, \mathbf{m}_h^0 \rangle \psi_j$.
 - 3: **for** $n = 0$ to $N - 1$ **do**
 - 4: Obtain coarse scale solution \mathbf{m}_H^{n+1} by solving (3.2).
 - 5: **end for**
-

Algorithm 2 Multiscale length preserving backward FEM for LL equation

- 1: Obtain the multiscale basis $\Psi = \{\psi_j\}_{j=1}^{N_H}$ by solving (3.1).
 - 2: Prescribe initial conditions $\mathbf{m}_h^0, \tilde{\mathbf{m}}_H^0 = \sum_j \langle \phi_j, \mathbf{m}_h^0 \rangle \psi_j$.
 - 3: **for** $n=0$ to $N-1$ **do**
 - 4: Projection onto unit sphere $\mathbf{m}_H^n = \frac{\tilde{\mathbf{m}}_H^n}{|\tilde{\mathbf{m}}_H^n|}$;
 - 5: Obtain the intermediate coarse scale solution $\tilde{\mathbf{m}}_H^{n+1}$ by solving (3.2).
 - 6: **end for**
 - 7: Projection onto unit sphere $\mathbf{m}_H^N = \frac{\tilde{\mathbf{m}}_H^N}{|\tilde{\mathbf{m}}_H^N|}$.
-

In Algorithm 2, it is important to note that the preservation of unit length on the fine scale is implied by $\mathbf{m}_H^n = \frac{\tilde{\mathbf{m}}_H^n}{|\tilde{\mathbf{m}}_H^n|}$ rather than projection step of coefficients on the coarse scale directly, with $\tilde{\mathbf{m}}_H^n$ indicates the fine scale intermediate solution. This choice is based on the fact that \mathbf{m}_H^n provides a good approximation of \mathbf{m}_h^n at the fine scale, while the direct division operation at the coarse scale eliminates the scaling factor c_e or c_τ , which will introduce issues in the subsequent time step evolution.

3.3 Speed-up Operation for Nonlinear Term Assembly

The assembly of nonlinear terms using classical FEM is a time-intensive process. For instance, the 4-valence tensor necessitates four iterations to traverse each fine simplex, as illustrated by the following equation:

$$(|\nabla \mathbf{m}_h^j|^2 \varphi_j, \varphi_i) = ((\sum_{k=1}^{N_h} \mathbf{m}_{h,k}^j \nabla \varphi_k) (\sum_{l=1}^{N_h} \mathbf{m}_{h,l}^j \nabla \varphi_l) \varphi_j, \varphi_i),$$

where $\varphi_i, \varphi_j, \varphi_k, \varphi_l \in V_h$ with $i, j, k, l = 1, \dots, N_h$. So as the 4-valence tensor for the anisotropic term $((\sum_{k=1}^{N_h} \mathbf{m}_{h,k}^j \nabla \varphi_k) (\sum_{l=1}^{N_h} \mathbf{m}_{h,l}^j \nabla \varphi_l) \varphi_j, \varphi_i)$. Besides, when dealing with a fourth-order polynomial, a minimum of a 6-point quadrature formula becomes essential.

The backward Euler schemes (6.1)-(6.5), particularly (6.2) and (6.3), enable computational acceleration through their square term incorporation. However, pre-computing the required 4-valence tensor in GRPS space exceeds practical memory limits due to dimensionality, which motivates us to transform the 4-valence tensor into a 3-valence tensor following [39].

For scheme (6.2) with GRPS bases, we seek $\mathbf{m}_H^{n+1} \in \mathbf{V}_H$ satisfying

$$A^n(\mathbf{m}_H^{n+1}, \mathbf{v}) = (\mathbf{f}_H^n, \mathbf{v}_H), \quad \forall \mathbf{v}_H \in \mathbf{V}_H. \quad (3.2)$$

Define the L^2 -projection $P_{GRPS}: H^1(\Omega) \rightarrow V_H$,

$$(P_{GRPS}(u), v) = (u, v), \quad \forall v \in V_H. \quad (3.3)$$

we propose an accelerated variant,

$$\begin{aligned} & (D_\tau \mathbf{m}_H^{n+1}, \mathbf{v}) + B^n(\mathbf{m}_H^{n+1}, \mathbf{v}) - (\mathbf{m}_H^n \times \mathbf{m}_{H,a}^{n+1}, \mathbf{v}) \\ & = \lambda(\kappa(\mathbf{x}) P_{GRPS}(|\nabla \mathbf{m}_H^n|^2) \mathbf{m}_H^{n+1}, \mathbf{v}) + \lambda(P_{GRPS}(|m_{H,2}^n|^2 + |m_{H,3}^n|^2) \mathbf{m}_H^{n+1}, \mathbf{v}). \end{aligned} \quad (3.4)$$

The acceleration stems from reduced assembly complexity,

$$(\kappa(\mathbf{x}) P_{GRPS}(|\nabla \mathbf{m}_H^n|^2) \mathbf{m}_H^{n+1}, \psi_l) = (\kappa(\mathbf{x}) \sum_{i,j=1}^{N_H} \rho_i^n \mathbf{m}_{H,j}^{n+1} \psi_i \psi_j, \psi_l). \quad (3.5)$$

Define tensor $\omega = (\omega_{kji})$ and vector $\mathbf{d} = (d_i)$,

$$\omega_{kji} = (\partial_x \psi_k \partial_x \psi_j + \partial_y \psi_k \partial_y \psi_j, \psi_i), \quad (3.6)$$

$$d_i = (|\nabla \mathbf{m}_H^n|^2, \psi_i). \quad (3.7)$$

The coefficients ρ_l^n solve the following linear system,

$$\mathbf{d} = M \rho^n, \quad M_{il} = (\psi_l, \psi_i). \quad (3.8)$$

The final assembly uses precomputed tensors ω and $\bar{\omega}$, both facilitating reusable computations, with analogous treatment for the anisotropy term $\bar{\omega}$:

$$\bar{\omega}_{kji} = (\psi_k \psi_j, \psi_i). \quad (3.9)$$

4 Numerical Experiments

We conduct numerical tests to evaluate our multiscale method's performance, specifically examining the variational formulation setup, treatment of the length-preserving step, and acceleration of nonlinear terms.

Experimental Setup All 2D simulations use $\Omega = [0,1]^2$ with $T = 1.0$. Initial conditions are $\mathbf{m}_0 = (1/\sqrt{2}, 1/\sqrt{3}, 1/\sqrt{6})^T$ with homogeneous Neumann boundary conditions and damping parameter $\lambda = 1$.

We measure solution accuracy using relative errors at final time T :

$$\frac{\|\mathbf{m}_h^N - \mathbf{m}_H^{l,N}\|}{\|\mathbf{m}_h^N\|}, \quad (4.1)$$

where $\|\cdot\|$ denotes H^1 norm, l is the localization level, and N represents the final time step.

Multiscale Coefficient We employ the oscillatory MsTrig coefficient:

$$\kappa(x,y) = \frac{1}{6} \left[\sum_{i=1}^5 f_i(x,y,\epsilon_i) + \sin(4x^2y^2) + 1 \right], \quad (4.2)$$

where $\epsilon_i = \{1/5, 1/13, 1/17, 1/31, 1/65\}$ and f_i are trigonometric terms (see Appendix 6.3). Figure 4.1 shows its highly oscillatory profile.

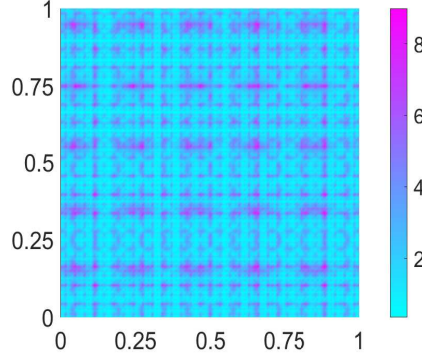


Figure 4.1: MsTrig coefficient $\kappa(x,y)$ on $\Omega = [0,1]^2$.

Following [50, 54, 58], we expect error bounds consistent with Theorem 2.1 when applying GRPS bases to the LL equation.

Key Parameters Key factors under examination:

- Basis variational forms (V1, V2);
- Measurement functions (E, V);
- Coarse time step choices ($\tau_H = H$ vs H^2);
- Length-preservation implementation.

4.1 Accuracy Tests: The Influence of the Key Parameters

We employ the schemes described in Appendix 6.1, as the length-preserving step has been rigorously justified theoretically. The non-separable multiscale coefficient (4.2) is used with final time T , spatial domain Ω , and damping parameter λ (T, Ω, λ) consistent with previous settings. The reference solution on a fine mesh uses $h = 1/2^7$ and $\Delta t = h^2$, while coarse grids are divided into $N_c = 2, 4, 8, 16$ ($H = 1/N_c$) with time steps $\tau_H = H, H^2$.

4.1.1 Without Length Preserving Step

The effective field $\mathbf{h}_{\text{eff}} = \text{div}(\kappa \nabla \mathbf{m}) - (\mathbf{m} - (\mathbf{m} \cdot \mathbf{u})\mathbf{u})$ remains crucial, as established by Landau and Lifshitz [43]. The multiscale basis from optimization problems (V1), (V2), and their combination maintains effectiveness with the anisotropy term.

In Tables 1-3, we record the global relative H^1 error convergence rates on a series of coarse degrees of freedoms when $N_c = 2, 4, 8, 16$ with diverse types of measurement functions, basis variational forms and coarse time steps. Upon examination of An's method, Cimrák's method, and Gao's method, it is observed that for coarse time steps $\tau_H = H, H^2$, both the proposed GRPS-E and GRPS-V methods converge with rates of 1 and 2, respectively. Given that the previous three methods exhibit first-order accuracy in time and at least first-order accuracy in space within the multiscale Finite Element Method (FEM) framework concerning H^1 norm (with $O(H^2)$ accuracy for GRPS-V), it is evident that the selection of coarse time steps could impact the spatial order. However, for GRPS-E, which exhibits higher order accuracy, this may be attributed to the super convergence phenomenon in this problem.

Table 1: $\kappa = \text{MsTrig}$. An's method. Global convergence rates comparing fine mesh reference solution to multiscale solution using GRPS-E and GRPS-V bases. TMB stands for "Type of multiscale bases," while TMF stands for "Type of measurement function." Fine mesh: $h = 1/2^7$, $\Delta t = h^2$. Coarse grid: $N_c = 2, 4, 8, 16$, $\tau_H = H, H^2$.

TMB \ TMF	Convergence Rate			
	GRPS-E, $\tau_H = H$	GRPS-E, $\tau_H = H^2$	GRPS-V, $\tau_H = H$	GRPS-V, $\tau_H = H^2$
(V1)+(V2)	-0.4182	-0.8187	-0.4643	-0.9940
(V1)	-0.4303	-0.9174	-0.4833	-0.9940
(V2)	-0.4172	-0.6646	-0.4833	-0.9941

Table 2: Cimrák's method. Global convergence rates without length preserving constraint. Parameters as in Table 1.

TMB \ TMF	Convergence Rate			
	GRPS-E, $\tau_H = H$	GRPS-E, $\tau_H = H^2$	GRPS-V, $\tau_H = H$	GRPS-V, $\tau_H = H^2$
(V1)+(V2)	-0.51730	-0.89267	-0.55234	-1.0325
(V1)	-0.51422	-0.95192	-0.52973	-1.0325
(V2)	-0.51675	-0.74907	-0.52672	-1.0210

Next, we compare the time-accuracy of GRPS-E and GRPS-V on a laptop with an Intel i9-14900HX CPU at $2.2\text{GHz} \times 32$ processors and 64GB of RAM running MATLAB version R2023a, as shown in Figure 4.2. Since the computation time is proportional to the degrees of freedom (dofs) of the coarse mesh, the time-accuracy table also exhibits the localization properties, similar to the dof-accuracy table, with the increasing number of

Table 3: Gao’s method. Global convergence rates without length preserving constraint. Parameters as in Table 1.

TMB	TMF	Convergence Rate			
		GRPS-E, $\tau_H = H$	GRPS-E, $\tau_H = H^2$	GRPS-V, $\tau_H = H$	GRPS-V, $\tau_H = H^2$
(V1)+(V2)		-0.44480	-0.86602	-0.48332	-0.99940
(V1)		-0.44427	-0.92084	-0.48332	-0.99940
(V2)		-0.44847	-0.73035	-0.48332	-0.99940

the localization parameter l from 3 to 8 in Figure 4.2.

To achieve nearly the same accuracy on both fine and coarse meshes, i.e., $h = H^2$, we set $\tau_H = H^2$ on the coarse scale to achieve $O(H^2)$ accuracy in the H^1 norm for spatial accuracy. Correspondingly, on the fine mesh, we set $\Delta t = h$ to attain $O(h)$ accuracy. Numerical results suggest that the reference solution ($h = 2^{-7}$, $\Delta t = h$) required 36 seconds (excluding the assembly of the 4-valence tensors, which is extremely time-consuming in nonlinear problems, focusing solely on solving the linear systems). In comparison, GRPS-E ($N_c = 16$) took 15.4 seconds (a reduction of 57.22%), and GRPS-V took 7.4 seconds (a reduction of 79.44%). Both GRPS-E and GRPS-V show significant efficiency improvements when employing the numerical scale-upscaling procedure. The main difference in computational time between GRPS-E and GRPS-V arises from the increased number of coarse degrees of freedom in GRPS-E compared to GRPS-V, resulting in higher computational costs.

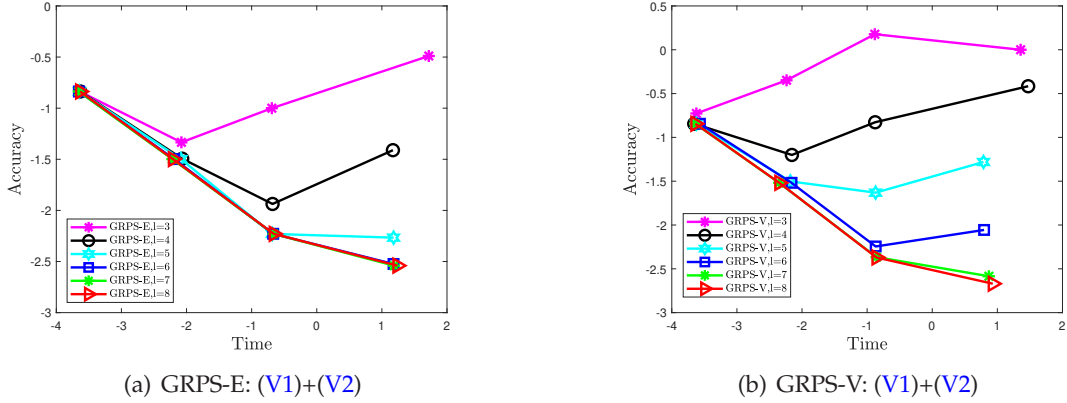


Figure 4.2: Performance of GRPS-E and GRPS-V multiscale bases solving (V1)+(V2) with localization levels $l = 3, 4, 5, 6, 7, 8$. X-axis: time (seconds), Y-axis: H^1 relative error (log10 scale).

4.1.2 With Length Preserving Step

Incorporating the unit length constraint (Algorithm 2) and exchange/anisotropy terms, we use coefficient (4.2) with $h=1/2^7$, $\Delta t=h^2$, and $N_c=2,4,8,16$ ($\tau_H=H, H^2$).

Table 4: An’s method. Global convergence rates with length preserving constraint. Parameters as in Table 1.

TMF \ TMB	Convergence Rate			
	GRPS-E, $\tau_H=H$	GRPS-E, $\tau_H=H^2$	GRPS-V, $\tau_H=H$	GRPS-V, $\tau_H=H^2$
(V1)+(V2)	-0.49115	-0.79407	-0.50260	-1.0028
(V1)	-0.46229	-0.92290	-0.50260	-1.0028
(V2)	-0.46230	-0.92312	-0.50260	-1.0028

Table 5: Cimrák’s method. Global convergence rates with length preserving constraint. Parameters as in Table 1.

TMF \ TMB	Convergence Rate			
	GRPS-E, $\tau_H=H$	GRPS-E, $\tau_H=H^2$	GRPS-V, $\tau_H=H$	GRPS-V, $\tau_H=H^2$
(V1)+(V2)	-0.46975	-0.72577	-0.50895	-0.99859
(V1)	-0.46830	-0.91898	-0.50895	-0.99859
(V2)	-0.46614	-0.91770	-0.50895	-0.99859

Table 6: Gao’s method. Global convergence rates with length preserving constraint. Parameters as in Table 1.

TMF \ TMB	Convergence Rate			
	GRPS-E, $\tau_H=H$	GRPS-E, $\tau_H=H^2$	GRPS-V, $\tau_H=H$	GRPS-V, $\tau_H=H^2$
(V1)+(V2)	-0.46185	-0.79233	-0.50260	-1.0028
(V1)	-0.46229	-0.92290	-0.50260	-1.0028
(V2)	-0.46230	-0.92313	-0.50260	-1.0028

In Tables 4-6, we employ length preserving Algorithm 2, we record the global relative H^1 error convergence rates on a range of coarse degrees of freedom when $N_c=2,4,8,16$ with diverse types of measurement functions, basis variational forms and coarse time steps. Similar to what was observed in Tables 1-3, Tables 4-6 illustrate that the proposed bases are all effective, and the global convergence rates remain consistent with those presented above, even without length preserving considerations.

Summary After solving the LL equation using various backward Euler schemes—including An’s method, Cimrák’s method, and Gao’s method — we observe that all methods achieve

the same order of accuracy and exhibit nearly identical computational efficiency when applied with different basis variational forms (Eqs. (V1) and (V2)). Additionally, as demonstrated in prior tests, the selection of coarse time steps can negatively impact the spatial error order.

Furthermore, proper enforcement of the length-preservation step does not significantly affect runtime but is crucial for maintaining the unit-length constraint. Regarding measurement functions, a comparison between GRPS-E and GRPS-V reveals that GRPS-V is computationally more efficient, as it requires fewer basis functions than GRPS-E, leading to reduced runtime.

4.2 The Performance of Speed-Up Operation

Since GRPS-V is more efficient than GRPS-E in terms of computational time, we compare the computational time between classical FEM and GRPS-V basis for equivalent H^1 error orders, using identical parameters from previous tests. Table 7 shows:

- CT0: Reference solution time (finest mesh);
- CT1: Fine matrix assembly (4-valence tensor, days) + CT0;
- CT2: Multiscale basis generation;
- CT3: 3-valence tensor assembly;
- CT4: Coarse scale solution time.

For coarse time step $\tau_H = H^2$, GRPS-V achieves second-order H^1 accuracy in space. At $N_c = 2^4$ ($h = H^2$), the multiscale approach matches FEM precision $O(h)$, resulting in a significant reduction in time from CT0 to CT4, greatly reducing runtime by $\geq 94.4\%$.

Table 7: Time comparison between standard (3.2) and accelerated (3.4) schemes in GRPS-V space. Parameters: $h = 1/2^8$, $\Delta t = h$; coarse grid $N_c = 2, 4, 8, 16$ with $\tau_H = H^2$.

$\begin{matrix} \text{Time} \\ \backslash \\ N_c \end{matrix}$	2	4	8	16
CT0 (s)	418	418	418	418
CT1 (Day)	3.1	3.1	3.1	3.1
CT2 (s)	0.176	1.225	9.414	27
CT3 (s)	673	3589	10573	14951
CT4 (s)	2.04e-4	6.81e-3	1.32e-1	6.99

Table 7 illustrates that the assembly of the finest 4-valence tensor (CT1) is significantly time and memory-intensive due to the curse of dimensionality. Implementing speed-up operations notably decreases both assembly time and memory requirements (CT3). CT2

indicates the generation of the GRPS-V bases, each of which is independent and can be solved concurrently. Furthermore, utilizing GRPS-V bases facilitates solving linear systems in a low-dimensional space, resulting in a significant reduction in time from CT0 to CT4. Finally, the speed-up operations achieve nearly the same level of accuracy as shown in Table 5. Therefore, a detailed display will not be provided here.

Remark 4.1. The accuracy of the accelerated scheme (3.4) is almost the same with the Tables 1-3 under examinations, and some related rigorous proofs are detailed in [39]. Hence, we will not include an excessive number of tables and instead focus solely on the performance of accelerated schemes.

5 Conclusion and Discussion

This paper presents a numerical homogenization method for solving the Landau-Lifshitz equation with rough coefficients. Our results demonstrate that when \mathbf{h}_{eff} includes an anisotropy term, both GRPS-E and GRPS-V multiscale bases obtained through minimization problems (V1) and (V2) effectively capture the essential information of the divergence-form operator.

From a physical perspective, the inclusion of anisotropy terms proves crucial for proper information extraction, consistent with the Landau-Lifshitz theory [43]. The model selection for the optimization problem significantly impacts our ability to compress operator information during multiscale basis construction. Computationally, our method achieves substantial efficiency gains compared to direct fine-mesh FEM solutions, while maintaining solution accuracy through coarse-mesh upscaling.

Future research directions will focus on three key aspects: First, establishing rigorous convergence analysis for the proposed method. Second, developing efficient numerical schemes for time-dependent coefficient cases. Third, extending the framework to handle more complex material configurations and boundary conditions.

Acknowledgments

ZM, RD and LZ were partially supported by the National Natural Science Foundation of China (Grant No. 12271360). LZ was also partially supported by the Fundamental Research Funds for the Central Universities. JC was partially supported by NSFC grant 12425113. The authors gratefully acknowledge Professor Rong An and Doctor Panchi Li for valuable discussions and insights.

References

- [1] Assyr Abdulle and Gilles Vilmart. Analysis of the finite element heterogeneous multiscale method for quasilinear elliptic homogenization problems. *Mathematics of Computation*, 83(286):513–536, 2014.

- [2] Grégoire Allaire and Robert Brizzi. A multiscale finite element method for numerical homogenization. *Multiscale Modeling & Simulation*, 4(3):790–812, 2005.
- [3] Francois Alouges. A new finite element scheme for Landau-Lifshitz equations. *Discrete & Continuous Dynamical Systems - S*, 1(2):187–196, 2008.
- [4] Francois Alouges, Anne De Bouard, Benoit Merlet, and Lea Nicolas. Stochastic homogenization of the Landau–Lifshitz–Gilbert equation. *Stochastics and Partial Differential Equations: Analysis and Computations*, 9:789–818, 2021.
- [5] Francois Alouges and Giovanni Di Fratta. Homogenization of composite ferromagnetic materials. *Proceedings of the Royal Society A: Mathematical, Physical and Engineering Sciences*, 471(2182):20150365, 2015.
- [6] Robert Altmann, Patrick Henning, and Daniel Peterseim. Numerical homogenization beyond scale separation. *Acta Numerica*, 30:1–86, 2021.
- [7] Rong An and Weiwei Sun. Analysis of backward Euler projection FEM for the Landau–Lifshitz equation. *IMA Journal of Numerical Analysis*, 42(3):2336–2360, 2022.
- [8] Todd Arbogast. Analysis of a two-scale, locally conservative subgrid upscaling for elliptic problems. *SIAM Journal on Numerical Analysis*, 42(2):576–598, 2004.
- [9] Y Bazilevs, VM Calo, JA Cottrell, TJR Hughes, A Reali, and G Scovazzi. Variational multi-scale residual-based turbulence modeling for large eddy simulation of incompressible flows. *Computer Methods in Applied Mechanics and Engineering*, 197(1):173–201, 2007.
- [10] Leonid Berlyand, Alexander G Kolpakov, and Alexei Novikov. *Introduction to the network approximation method for materials modeling*. Number 148 in Encyclopedia of Mathematics and its Applications. Cambridge University Press, 2013.
- [11] Leonid Berlyand and Houman Owhadi. Flux norm approach to finite dimensional homogenization approximations with non-separated scales and high contrast. *Archive for rational mechanics and analysis*, 198(2):677–721, 2010.
- [12] Francesca Bonizzoni, Philip Freese, and Daniel Peterseim. Super-localized orthogonal decomposition for convection-dominated diffusion problems. *BIT Numerical Mathematics*, 64(3):33, 2024.
- [13] Francesca Bonizzoni, Moritz Hauck, and Daniel Peterseim. A reduced basis super-localized orthogonal decomposition for reaction-convection-diffusion problems. *Journal of Computational Physics*, 499:112698, 2024.
- [14] Yongyong Cai, Jingrun Chen, Cheng Wang, and Changjian Xie. A second-order numerical method for Landau-Lifshitz-Gilbert equation with large damping parameters. *Journal of Computational Physics*, 451:110831, 2022.
- [15] Carlos J García Cervera. Numerical micromagnetics: a review. *SeMA Journal: Boletín de la Sociedad Española de Matemática Aplicada*, (39):103–135, 2007.
- [16] Jingrun Chen, Rui Du, Zetao Ma, Zhiwei Sun, and Lei Zhang. On the Multiscale Landau–Lifshitz–Gilbert Equation: Two-Scale Convergence and Stability Analysis. *Multiscale Modeling & Simulation*, 20(2):835–856, 2022.
- [17] Ya-Zhe Chen and Lan-Cheng Wu. *Second order elliptic equations and elliptic systems*, volume 174. American Mathematical Soc., 1998.
- [18] Catherine Choquet, Mohammed Moumni, and Mouhcine Tilioua. Homogenization of the Landau-Lifshitz-Gilbert equation in a contrasted composite medium. *Discrete & Continuous Dynamical Systems-S*, 11(1):35, 2018.
- [19] Eric T Chung, Yalchin Efendiev, and Wing Tat Leung. Residual-driven online generalized multiscale finite element methods. *Journal of Computational Physics*, 302:176–190, 2015.
- [20] Eric T Chung, Yalchin Efendiev, and Wing Tat Leung. An adaptive generalized multiscale

- discontinuous galerkin method for high-contrast flow problems. *Multiscale Modeling & Simulation*, 16(3):1227–1257, 2018.
- [21] Eric T Chung, Yalchin Efendiev, and Guanglian Li. An adaptive GMSFEM for high-contrast flow problems. *Journal of Computational Physics*, 273:54–76, 2014.
 - [22] Ivan Cidrák. Error estimates for a semi-implicit numerical scheme solving the Landau–Lifshitz equation with an exchange field. *IMA Journal of Numerical Analysis*, 25(3):611–634, 2005.
 - [23] Ivan Cidrák. A survey on the numerics and computations for the landau-lifshitz equation of micromagnetism. *Archives of Computational Methods in Engineering*, 15(3):1–37, 2007.
 - [24] Giovanni Di Fratta, Carl-Martin Pfeiler, Dirk Praetorius, Michele Ruggeri, and Bernhard Stifter. Linear second-order IMEX-type integrator for the (eddy current) Landau–Lifshitz–Gilbert equation. *IMA Journal of Numerical Analysis*, 40(4):2802–2838, 2020.
 - [25] Christian Döding, Patrick Henning, and Johan Wärnegard. A two level approach for simulating Bose-Einstein condensates by localized orthogonal decomposition. *arXiv preprint arXiv:2212.07392*, 2022.
 - [26] Louis J Durlofsky. Numerical calculation of equivalent grid block permeability tensors for heterogeneous porous media. *Water resources research*, 27(5):699–708, 1991.
 - [27] Weinan E and Bjorn Engquist. The heterogeneous multiscale methods. *Communications in Mathematical Sciences*, 1(1):87–132, 2003.
 - [28] Weinan E, Pingbing Ming, and Pingwen Zhang. Analysis of the heterogeneous multiscale method for elliptic homogenization problems. *Journal of the American Mathematical Society*, 18(1):121–156, 2005.
 - [29] Yalchin Efendiev, Juan Galvis, and Thomas Y Hou. Generalized multiscale finite element methods (GMSFEM). *Journal of Computational Physics*, 251:116–135, 2013.
 - [30] Yalchin Efendiev, Juan Galvis, and Xiao-Hui Wu. Multiscale finite element methods for high-contrast problems using local spectral basis functions. *Journal of Computational Physics*, 230(4):937–955, 2011.
 - [31] Yalchin Efendiev and Thomas Y Hou. *Multiscale finite element methods: theory and applications*, volume 4. Springer Science & Business Media, 2009.
 - [32] Philip Freese, Dietmar Gallistl, Daniel Peterseim, and Timo Sprekeler. Computational multiscale methods for nondivergence-form elliptic partial differential equations. *Computational Methods in Applied Mathematics*, 24(3):649–672, 2024.
 - [33] Dietmar Gallistl, Patrick Henning, and Barbara Verfürth. Numerical homogenization of $h(\text{curl})$ -problems. *SIAM Journal on Numerical Analysis*, 56(3):1570–1596, 2018.
 - [34] Huadong Gao. Optimal error estimates of a linearized backward Euler FEM for the Landau–Lifshitz equation. *SIAM Journal on Numerical Analysis*, 52(5):2574–2593, 2014.
 - [35] Thomas L Gilbert. A Lagrangian formulation of the gyromagnetic equation of the magnetization field. *Phys. Rev.*, 100:1243–1255, 1955.
 - [36] Oliver Gutfleisch, Matthew A Willard, Ekkes Brück, Christina H Chen, SG Sankar, and J Ping Liu. Magnetic materials and devices for the 21st century: stronger, lighter, and more energy efficient. *Advanced materials*, 23(7):821–842, 2011.
 - [37] Moritz Hauck and Daniel Peterseim. Super-localization of elliptic multiscale problems. *Mathematics of Computation*, 92(341):981–1003, 2023.
 - [38] Patrick Henning and Anna Persson. Computational homogenization of time-harmonic Maxwell’s equations. *SIAM Journal on Scientific Computing*, 42(3):B581–B607, 2020.
 - [39] Patrick Henning and Johan Wärnegard. Superconvergence of time invariants for the Gross–Pitaevskii equation. *Mathematics of Computation*, 91(334):509–555, 2022.

- [40] Thomas JR Hughes, Gonzalo R Feijóo, Luca Mazzei, and Jean-Baptiste Quinicy. The variational multiscale method—a paradigm for computational mechanics. *Computer methods in applied mechanics and engineering*, 166(1-2):3–24, 1998.
- [41] Vasili Vasilievitch Jikov, Sergei M Kozlov, and Olga Arsenievna Oleinik. *Homogenization of differential operators and integral functionals*. Springer Science & Business Media, 2012.
- [42] Martin Kruzik and Andreas Prohl. Recent developments in the modeling, analysis, and numerics of ferromagnetism. *SIAM review*, 48(3):439–483, 2006.
- [43] L. D. Landau and E. M. Lifshitz. On the theory of the dispersion of magnetic permeability in ferromagnetic bodies. *Phys. Z. Sowjetunion*, 8:153–169, 1935.
- [44] Lena Leitenmaier. *Analysis and numerical methods for multiscale problems in magnetization dynamics*. PhD thesis, KTH Royal Institute of Technology, 2021.
- [45] Lena Leitenmaier and Murtazo Nazarov. A finite element based Heterogeneous Multiscale Method for the Landau-Lifshitz equation. *Journal of Computational Physics*, 486:112112, 2023.
- [46] Lena Leitenmaier and Olof Runborg. Heterogeneous Multiscale Methods for the Landau-Lifshitz Equation. *Journal of Scientific Computing*, 93(3):76, 2022.
- [47] Lena Leitenmaier and Olof Runborg. On homogenization of the Landau-Lifshitz equation with rapidly oscillating material coefficient. *Communications in Mathematical Sciences*, 20(3):653–694, 2022.
- [48] Lena Leitenmaier and Olof Runborg. Upscaling Errors in Heterogeneous Multiscale Methods for the Landau-Lifshitz Equation. *Multiscale Modeling & Simulation*, 20(1):1–35, 2022.
- [49] Xinliang Liu, Eric Chung, and Lei Zhang. Iterated numerical homogenization for multiscale elliptic equations with monotone nonlinearity. *Multiscale Modeling & Simulation*, 19(4):1601–1632, 2021.
- [50] Xinliang Liu, Lei Zhang, and Shengxin Zhu. Generalized Rough Polyharmonic Splines for Multiscale PDEs with Rough Coefficients. *Numerical Mathematics: Theory, Methods and Applications*, 14(4):862–892, 2021.
- [51] Chupeng Ma, Robert Scheichl, and Tim Dodwell. Novel design and analysis of generalized finite element methods based on locally optimal spectral approximations. *SIAM Journal on Numerical Analysis*, 60(1):244–273, 2022.
- [52] Roland Maier and Barbara Verfürth. Multiscale scattering in nonlinear Kerr-type media. *Mathematics of Computation*, 91(336):1655–1685, 2022.
- [53] Axel Målqvist and Daniel Peterseim. Localization of elliptic multiscale problems. *Mathematics of Computation*, 83(290):2583–2603, 2014.
- [54] Houman Owhadi. Multigrid with rough coefficients and multiresolution operator decomposition from hierarchical information games. *Siam Review*, 59(1):99–149, 2017.
- [55] Houman Owhadi and Lei Zhang. Homogenization of parabolic equations with a continuum of space and time scales. *SIAM Journal on Numerical Analysis*, 46(1):1–36, 2008.
- [56] Houman Owhadi and Lei Zhang. Localized bases for finite-dimensional homogenization approximations with nonseparated scales and high contrast. *Multiscale Modeling & Simulation*, 9(4):1373–1398, 2011.
- [57] Houman Owhadi and Lei Zhang. Gamblets for opening the complexity-bottleneck of implicit schemes for hyperbolic and parabolic odes/pdes with rough coefficients. *Journal of Computational Physics*, 347:99–128, 2017.
- [58] Houman Owhadi, Lei Zhang, and Leonid Berlyand. Polyharmonic homogenization, rough polyharmonic splines and sparse super-localization. *ESAIM: Mathematical Modelling and Numerical Analysis*, 48(2):517–552, 2014.
- [59] George Papanicolau, Alain Bensoussan, and J-L Lions. *Asymptotic analysis for periodic struc-*

tures. Elsevier, 1978.

- [60] Dirk Praetorius, Michele Ruggeri, and Bernhard Stiffner. Convergence of an implicit–explicit midpoint scheme for computational micromagnetics. *Computers & Mathematics with Applications*, 75(5):1719–1738, 2018.
- [61] Andreas Prohl et al. *Computational micromagnetism*. Springer, 2001.
- [62] K evin Santugini-Repiquet. Homogenization of ferromagnetic multilayers in the presence of surface energies. *ESAIM: Control, Optimisation and Calculus of Variations*, 13(2):305–330, 2007.
- [63] Barbara Verf urth. Numerical homogenization for nonlinear strongly monotone problems. *IMA Journal of Numerical Analysis*, 42(2):1313–1338, 2022.
- [64] Xiao-Hui Wu, Yalchin Efendiev, and Thomas Y Hou. Analysis of upscaling absolute permeability. *Discrete and Continuous Dynamical Systems Series B*, 2(2):185–204, 2002.
- [65] Changjian Xie, Carlos J Garc a-Cervera, Cheng Wang, Zhennan Zhou, and Jingrun Chen. Second-order semi-implicit projection methods for micromagnetics simulations. *Journal of Computational Physics*, 404:109104, 2020.

6 Appendix

6.1 Various Time Discretization Schemes

Prohl’s method The fully implicit scheme proposed by Prohl [61] ensures numerical stability through complete nonlinear treatment:

$$\frac{1}{\Delta t}(\mathbf{m}_h^{n+1} - \mathbf{m}_h^n, \mathbf{v}_h) - \lambda(\mathbf{h}_{\text{eff}}^{n+1}, \mathbf{v}_h) + (\mathbf{m}_h^{n+1} \times \mathbf{h}_{\text{eff}}^{n+1}, \mathbf{v}_h) = -\lambda((\mathbf{m}_h^n \cdot \mathbf{h}_{\text{eff}}^n) \cdot \mathbf{m}_h^{n+1}, \mathbf{v}_h), \quad (6.1)$$

for all $\mathbf{v}_h \in \mathbf{V}_h$ and $n = 0, 1, \dots, N-1$. This formulation requires nonlinear solvers at each time step.

Cimr k’s method Cimr k [22] developed a semi-implicit variant by linearizing the cross product term:

$$\frac{1}{\Delta t}(\mathbf{m}_h^{n+1} - \mathbf{m}_h^n, \mathbf{v}_h) - \lambda(\mathbf{h}_{\text{eff}}^{n+1}, \mathbf{v}_h) + (\mathbf{m}_h^n \times \mathbf{h}_{\text{eff}}^{n+1}, \mathbf{v}_h) = -\lambda((\mathbf{m}_h^n \cdot \mathbf{h}_{\text{eff}}^n) \cdot \mathbf{m}_h^{n+1}, \mathbf{v}_h). \quad (6.2)$$

This modification yields a linear system solvable without iteration, significantly improving computational efficiency while maintaining stability.

Gao’s method Gao [34] further simplified the right-hand side treatment:

$$\frac{1}{\Delta t}(\mathbf{m}_h^{n+1} - \mathbf{m}_h^n, \mathbf{v}_h) - \lambda(\mathbf{h}_{\text{eff}}^{n+1}, \mathbf{v}_h) + (\mathbf{m}_h^n \times \mathbf{h}_{\text{eff}}^{n+1}, \mathbf{v}_h) = -\lambda((\mathbf{m}_h^n \cdot \mathbf{h}_{\text{eff}}^n) \cdot \mathbf{m}_h^n, \mathbf{v}_h). \quad (6.3)$$

This scheme achieves optimal L^2 and H^1 error estimates without restrictive time-step conditions ($\Delta t = O(h^\alpha)$). The unit length constraint relaxation yields:

$$\|1 - |\mathbf{m}_h^n|^2\|_{L^2} \leq C_0(\Delta t + h^2), \quad (6.4)$$

demonstrating controlled deviation from the unit sphere.

An's method An [7] introduced a projection-based approach:

$$\frac{1}{\Delta t}(\tilde{\mathbf{m}}_h^{n+1} - \mathbf{m}_h^n, \mathbf{v}_h) - \lambda(\mathbf{h}_{\text{eff}}^{n+1}, \mathbf{v}_h) + (\mathbf{m}_h^n \times \mathbf{h}_{\text{eff}}^{n+1}, \mathbf{v}_h) = -\lambda((\mathbf{m}_h^n \cdot \bar{\mathbf{h}}_{\text{eff}}^{n+1}) \cdot \mathbf{m}_h^n, \mathbf{v}_h) \quad (6.5)$$

with post-processing projection step $\mathbf{m}_h^{n+1} = \tilde{\mathbf{m}}_h^{n+1} / |\tilde{\mathbf{m}}_h^{n+1}|$, and $\bar{\mathbf{h}}_{\text{eff}}^{n+1} = \nabla \tilde{\mathbf{m}}_h^{n+1} \cdot \kappa \nabla \mathbf{m}_h^n + \lambda \tilde{\mathbf{m}}_h^{n+1} \cdot \mathbf{m}_{h,a}^n$. While theoretically requiring $\Delta t = O(\epsilon_0 h)$ and $\mathbf{m}_0 \in H^{r+1}$ ($r \geq 2$), numerical experiments show these conditions can be relaxed.

6.2 Measurement Function Types

Let the set of edge-based measurement functions be denoted by $\Phi_{\mathcal{E}} = \{\phi_e\}_{e \in \mathcal{E}_H}$ and the set of volume-based measurement functions by $\Phi_{\mathcal{T}} = \{\phi_\tau\}_{\tau \in \mathcal{T}_H}$. The GRPS framework mainly employs two primary measurement function types:

- **Edge-based (Case E):** For $e \in \mathcal{E}_H$,

$$\phi_e = |e|^{\frac{2-d}{2(d-1)}} \chi(e), \quad \langle \phi_e, u \rangle = \int_e u dS; \quad (6.6)$$

- **Volume-based (Case V):** For $\tau \in \mathcal{T}_H$,

$$\phi_\tau = \sqrt{|\tau|} \chi(\tau), \quad \langle \phi_\tau, u \rangle = \sqrt{|\tau|} \int_\tau u dx, \quad (6.7)$$

where χ denotes characteristic functions and $|\cdot|$ the geometric measure.

6.3 The multiscale trigonometric (MsTrig) coefficient

The functions in (4.2) is defined by

- $f_1(x, y, \epsilon_1) = \frac{1.1 + \sin(2\pi x / \epsilon_1)}{1.1 + \sin(2\pi y / \epsilon_1)},$
- $f_2(x, y, \epsilon_2) = \frac{1.1 + \sin(2\pi y / \epsilon_2)}{1.1 + \cos(2\pi x / \epsilon_2)},$
- $f_3(x, y, \epsilon_3) = \frac{1.1 + \cos(2\pi x / \epsilon_3)}{1.1 + \sin(2\pi y / \epsilon_3)},$
- $f_4(x, y, \epsilon_4) = \frac{1.1 + \sin(2\pi y / \epsilon_4)}{1.1 + \cos(2\pi x / \epsilon_4)},$
- $f_5(x, y, \epsilon_5) = \frac{1.1 + \cos(2\pi x / \epsilon_5)}{1.1 + \sin(2\pi y / \epsilon_5)},$

where $\epsilon_1 = 1/5$, $\epsilon_2 = 1/13$, $\epsilon_3 = 1/17$, $\epsilon_4 = 1/31$, $\epsilon_5 = 1/65$.